JOURNAL OF THERMOPHYSICS AND HEAT TRANSFER
Vol. 25, No. 3, July–September 2011

Heat Transfer Through Single Hole Bias Flow Acoustic Liner

Anthony O. Ives,* Jian Wang,† and Srinivasan Raghunathan‡
Queen's University Belfast, Belfast, Northern Ireland BT7 1NN, United Kingdom
and
Patrick Sloan§
Bombardier Aerospace, Belfast, Northern Ireland BT3 9DZ, United Kingdom

DOI: 10.2514/1.T3637

Because of the political awareness of environmental damage, noise control legalization is a future problem facing industrial leaders. However, aircraft ice protection systems are essential for airworthiness requirements. As a result, modern technology is expected to perform multiple tasks. This paper investigates the heat transfer characteristics and mechanisms of an acoustic liner with bias flow. An idealized version of the acoustic liner is tested experimentally in the low-speed wind tunnel at Queens University, Belfast. Then, a numerical model is created for a single cell of the honeycomb structure in order to characterize the main heat transfer mechanisms. The simulation results are compared with the experimental measurements. Comparison between numerical solution and experiment show good agreement for heat transfer characteristics. The phenomena demonstrated by the single hole model are used to explain the heat transfer mechanisms of the bias acoustic liners. A higher heat transfer rate than expected is achieved which is verified both by numerical solution and experiment results. The primary reason for a higher heat transfer rate is due to an increase in heat transfer in the region where the flow inside each of the honeycomb cells reattaches to the sidewalls after exiting a small hole.

Nomenclature

A	=	local active area, m^2
A_{liner}	=	acoustic liner front face area, m^2
c_p	=	heat capacity of air at constant pressure, $J\,Kg^{-1}\,K^{-1}$
D	=	hydraulic diameter of honeycomb cells, m
d	=	hole diameter, m
F	=	shape factor for honeycomb wall
h	=	heat transfer coefficient
h_{BP}	=	back plate heat transfer coefficient
h_{EC}	=	heat transfer coefficient based on liner effective conductivity
h_{FD}	=	heat transfer coefficient for fully developed duct flow
h_{FP}	=	front plate heat transfer coefficient
h_{HC}	=	equivalent heat transfer coefficient for conduction
h_{liner}	=	heat transfer coefficient of acoustic liner
k_{air}	=	conductivity of air, $W\,m^{-1}\,K^{-1}$
k_e	=	effective conductivity for honeycomb materials, $W\,m^{-1}\,K^{-1}$
l	=	length of honeycomb cells, m
l_{char}	=	characteristic length of acoustic liner sample, m
l_{sample}	=	distance between leading edge and sample center, m
$\dot{m}$	=	mass flow rate of heated air, $kg\,s^{-1}$
$Nu_{A/P}$	=	Nusselt number with A/P reference value
P	=	hole pitch, m
q_{liner}	=	heat loss across acoustic liner, W
Re	=	Reynolds number
$Re_{A/P}$	=	Reynolds number with A/P reference value
T_{BH}	=	static temperature at back hole, K
T_{BP}	=	static temperature at back plate, K
T_{ex}	=	static temperature at freestream, K
T_{FH}	=	static temperature at front hole, K
T_{FP}	=	static temperature at front plate, K
T_{in}	=	static temperature downstream of porous plate, K
u	=	velocity in horizontal or x direction, ms^{-1}
U_{WT}	=	velocity in wind tunnel, ms^{-1}
U_∞	=	velocity in freestream in x direction, ms^{-1}
v	=	velocity in vertical or y direction, ms^{-1}
V_{in}	=	velocity downstream of porous plate in y direction, ms^{-1}
y	=	vertical position, m
Δp	=	pressure loss, Pa
ζ	=	normalized pressure
μ	=	dynamic viscosity of fluid, Pas
ρ	=	density, kgm^{-3}
ρ_∞	=	density of freestream air, kgm^{-3}
σ_{BP}	=	back plate porosity
σ_{FP}	=	front plate porosity

Received 8 October 2010; revision received 26 January 2011; accepted for publication 12 March 2011.

*Ph.D. Student, School of Mechanical and Aerospace Engineering.
†Lecturer, School of Mechanical and Aerospace Engineering; currently, Principal Lecturer, Faculty of Engineering, Kingston University, London, England SW15 3DW, United Kingdom. Senior Member AIAA.
‡Professor, School of Mechanical and Aerospace Engineering. Fellow AIAA.
§Project Engineer.

I. Introduction

IN RECENT times, there has been an emphasis in the media on environmental damage, drawing the attention of politicians and government. This usually results in current environmental protection legalization being tightened up, creating a new challenge for industrial leaders. At the same time, performance and other functions have to be sustained or improved. For example, when a noise reduction issue has to be addressed, anti/deicing certification has to be maintained. As a result, current technology needs to be improved to perform a wider range of tasks. This paper investigates the feasibility of the bias acoustic liner as a heat transfer medium and its working mechanism. The bias liner is particularly useful when both heat transfer and noise reduction are required, such as combustion chambers, nacelle intake anti/deicing, and jet engine nozzles. The bias liner was originally conceived to control combustion instabilities in combustion chambers and to cool the chamber wall.

The conventional acoustic liner currently used by industry is basically a honeycomb structure sandwiched between a porous plate and a nonporous plate, shown in Fig. 1.

The bias liner differs from the conventional acoustic liner, in that both plates are porous, illustrated in Fig. 2. A pressure difference across the two sides of this liner causes air to flow through it.

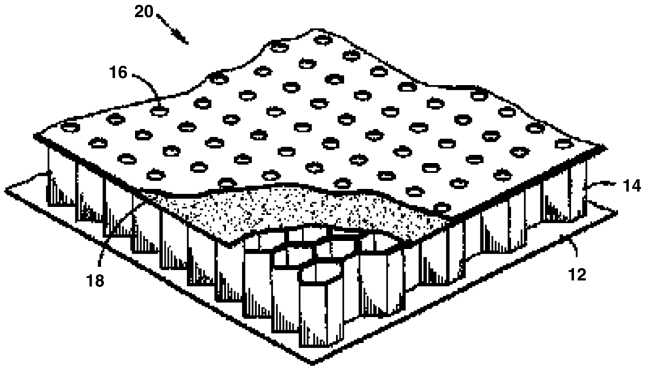

Fig. 1 Convectional acoustic liner [36].

The acoustic characteristics of the bias liner were first investigated by Dean and Tester [1]. Dean and Tester's work was limited to proof of concept, in which they found that a steady airflow does produce significant changes in acoustic properties of a liner. Since Dean and Tester, a number of other researchers have investigated the bias liner concept [2–4]. Sun et al. investigated the combined effects of grazing and bias flow, which leads to an empirical expression showing that grazing flow does have an influence on the liner acoustic properties [2]. However, the bias flow produces a stronger influence on acoustic absorption, demonstrated by Sun et al. [2]. Eldredge and Dowling looked at the more specific effect of the bias liner absorbing axial acoustic waves, deriving a complex mathematical model that was validated with experimental work [3]. Rademaker and Demmenie also developed an improved empirical model for the bias liner acoustic absorption properties [4].

Heat transfer across honeycomb structures has also been researched [5–7]. Swann and Pitman developed a semiempirical equation to calculate both radiation and conductive heat transfer in honeycomb-core and corrugated-core structure sandwich panels; this equation is widely accepted by industry [5]. Daryabeigi [6] evaluated the effect of adhesive on the Swann and Pitman model [5] through experiment, finding that the adhesive gives an increase in heat transfer. Lu investigated thermal conduction in the honeycomb cell perpendicular to an airflow blowing through the honeycomb cells. His work [6] used an extension of fin theory to mathematically model the thermal conduction in the honeycomb walls [7]. Lu validated his model using experimental work [7]. Natural convection properties in a hexagonal honeycomb-core sandwiched between two solid plates have also been investigated by Asako et al. using an unsteady numerical method [8]. Asako et al. found natural convection in a honeycomb cell gives, as expected, an unsteady flow pattern, but the flow pattern was symmetrical.

Heat transfer between porous plates and airflow has been studied by a range of researchers [9–11]. Sparrow and Ortiz first investigated heat transfer to porous plates using an experimental study and developed an empirical equation [9]. Kutscher also experimentally investigated heat transfer to porous plates; however, for lower velocities and the effects of crossflow, he also developed some empirical equations from his results [10]. Dorignac et al. performed a more detailed study looking at the effects of hole spacing and holes of smaller diameters, and they developed a more comprehensive empirical equation [11]. Research looking in more detail at heat transfer in the hole region has been carried out by Cho and Goldstein [12] and Cho et al. [13]; they developed a number of empirical equations for local heat transfer in various different regions of the hole [12,13].

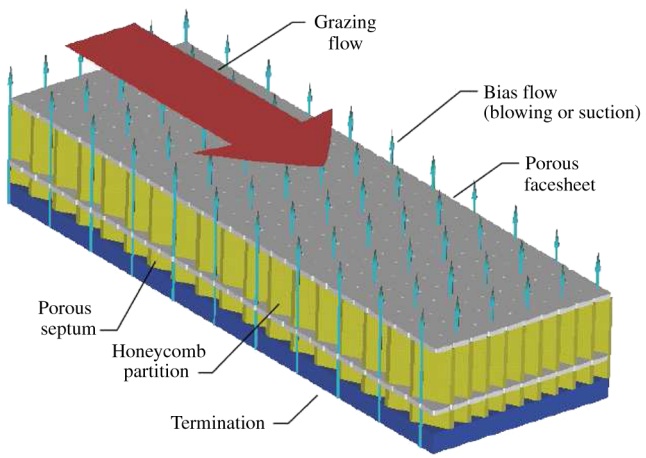

Fig. 2 Bias flow acoustic liner [37].

There have been a number of publications on pressure losses across porous plates, abrupt expansions, and contractions [10,14,15]. Kutscher found that, as hole size decreases, the pressure loss across the plate increases significantly due to viscous forces [10]. Kutscher developed an empirical equation that shows a dependence of pressure loss across the porous plate on Reynolds number [10]. Gan and Riffat compared a numerical study to that of an experimental study for pressure loss across a porous plate [14]. Gan and Riffat found that numerical methods can predict pressure loss coefficient across porous plates, and the hole geometry can be simplified without affecting the accuracy of results. Marjanovic and Djordjevic derived equations for changes in fluid properties of subsonic flow across abrupt expansions and contractions [15]. Broach et al. also found that hole inlet and outlet geometry can have a significant effect on pressure loss across porous plates [16].

Heat transfer to sidewalls after an abrupt expansion has also been studied and published [17–21]. Krall and Sparrow investigated the heat transfer in regions of separation, reattachment, and redevelopment of flow downstream of an abrupt expansion [17]. Krall and Sparrow's findings show that, at the point of reattachment, heat transfer was three to nine times that of corresponding fully developed flows [17]. Zemanick and Dougall's results also show that local heat transfer coefficients downstream of the expansion were always higher than the fully developed flow [18]. Zemanick and Dougall produced an expression for the maximum Nusselt number from their experimental results [18]. Amano carried out a numerical study of turbulent flow downstream of an abrupt expansion and then made a comparison with experiment results [19]. Baughn et al. carried out an experimental study of heat transfer downstream of abrupt expansion, both for the case of constant wall temperature and the case of constant wall flux [20,21]. Their results again showed an increase in heat transfer at the point of reattachment after an abrupt expansion [20].

However, with regard to heat transfer characteristics of an acoustic liner, a thorough review only found research work by Wong et al. [22,23] on the conventional acoustic liner. Wong et al. investigated the effect of the acoustic resonation on the liner heat transfer capability, showing that the effect was negligible [22]. They also found that the heat transfer properties of the acoustic liner were not as poor as had been expected [23].

A thorough literature review has revealed no research looking specifically at the heat transfer properties of the bias liner. The present paper will examine, both experimentally and numerically, the heat transfer and pressure loss characteristics of an idealized bias flow acoustic liner. The results will be discussed in order to establish an understanding of the heat transfer mechanisms.

II. Methods

Both experimental measurement and numerical modeling techniques have been conducted in this research. Heat transfer measurement of a simplified ideal bias liner was conducted in a low-speed wind tunnel to observe the behavior of heat transfer of the bias liner. Furthermore, a single honeycomb cell was modeled using Fluent® to enhance understanding of the heat transfer mechanisms.

A. Experimental Setup

A sample of a simplified acoustic liner was prepared with one hole on top and bottom plates in the center of the honeycomb cell. The sample was then tested, and measurements of pressure and

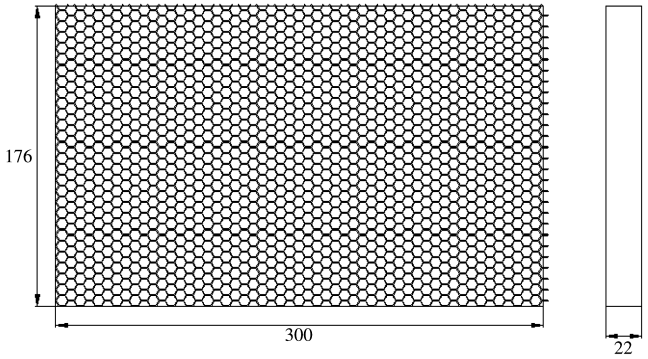

Fig. 3 Honeycomb-core dimensions (in mm).

temperature were taken in order to calculate heat transfer coefficients and pressure loss across the bias liner.

1. Sample Preparation

The acoustic liner sample was 300 mm in breadth and 176 mm in length. The sample was constructed from aluminum facing (external) and backing (internal) sheets of 1 mm and an aluminum honeycomb core of approximately 22 mm in height. Figure 3 shows honeycomb-core dimensions. The individual honeycomb cell has a width of approximately of 6.35 mm, a breadth of 7.33, and a wall thickness of 0.3 mm, as shown in Fig. 4.

The experiment is a controlled test for an idealized version of the acoustic bias liner, with one larger hole in each honeycomb cell on the front-covering sheet and one smaller hole on the back-covering sheet. Because of the large number of honeycomb cells and holes involved, alignment of the larger hole, honeycomb cell, and smaller hole presents a big challenge to manufacturing the sample. Special care has to be taken.

To guarantee the quality of the sample, the first stage in the liner manufacture was to bond the back sheet only to one side of the honeycomb core. Bonding was carried out in an autoclave at a temperature of 177°C, with a vacuum, and under applied pressure. The next stage was to drill the backing sheet. The backing sheet hole pattern for the sample was a 0.7 mm hole diameter at a pitch of approximately 6.35 mm along the length and approximately 7.33 mm hole pitch along the breadth. That would guarantee one hole per honeycomb cell to give a backing sheet porosity of 1%. A computer numerical control machine was used to drill the holes. However, since the operator had to periodically recenter the drill to ensure that all the holes were drilled in the cell center, only one side of the honeycomb cell was covered, making periodic recenter possible.

After the drilling process had been completed, the facing sheet without holes was bonded to the honeycomb using the same techniques as used for bonding the backing sheet. The cell center positions were known from the first drilling process; hence, this information was used to drill the larger holes on the facing sheet with a given pattern.

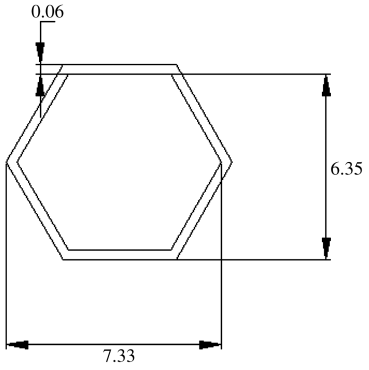

Fig. 4 Honeycomb cell dimensions (in mm).

The hole pattern for the facing sheet was a hole diameter of 2 mm with a hole pitch of approximately 6.35 mm along the length and approximately a 7.33 mm hole pitch along the breadth. That is one hole per honeycomb cell to give a facing sheet porosity of 9%.

2. Experimental Testing

Testing of the sample was carried out in a closed-circuit low-speed wind tunnel. The wind tunnel was capable of maximum velocity of 50 ms^{-1} with an effective working section of approximately 1.14×0.86 m.

A rig that consisted of Perspex plate with side supports, also made of Perspex, was installed in the wind tunnel. The Perspex plate was a length of 1315 mm and breadth of 700 mm, with a thickness of 25 mm. The rig itself had a cutout made in which the sample was placed. The dimensions of the cutout were 176×308 mm; again, it was 25 mm deep. The cutout for the sample was 879 mm from the Perspex plate leading edge.

Figure 5 shows the dimensions of the rig and the position of the cutout. For a wind-tunnel velocity of 30 ms^{-1}, this gives a Reynolds number of 1.9×10^6:

$$Re = \frac{\rho_\infty U_\infty l_{\text{char}}}{\mu} = \frac{\rho U_{\text{WT}} l_{\text{sample}}}{\mu} \tag{1}$$

where Re is the Reynolds number, ρ is the density, ρ_∞ is the freestream density, U_{WT} is the velocity in the wind tunnel, U_∞ is the freestream velocity, l_{char} is the characteristic length, and l_{sample} is the distance of the sample from the leading edge of the rig.

Figures 6 and 7 show experimental setup and apparatus. Four pressure tapings were placed in the Perspex plate in order to confirm that there was no pressure gradient across the plate. The blower fan could only be turned on or off; hence, a regulator valve was used to vary hot air flow rate.

The bias flow air was first passed through a 3 kW heater, and then through the test sample. The bias flow could be heated to

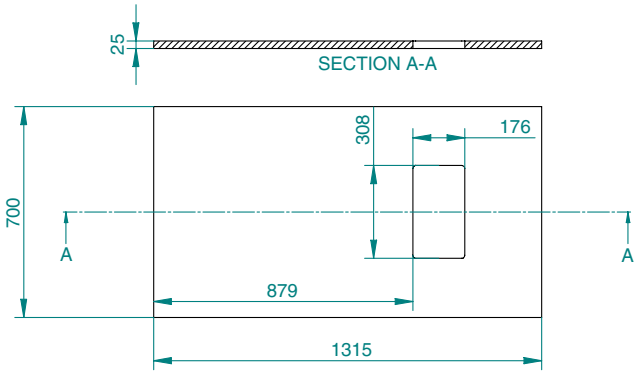

Fig. 5 Experimental rig with dimensions (in mm).

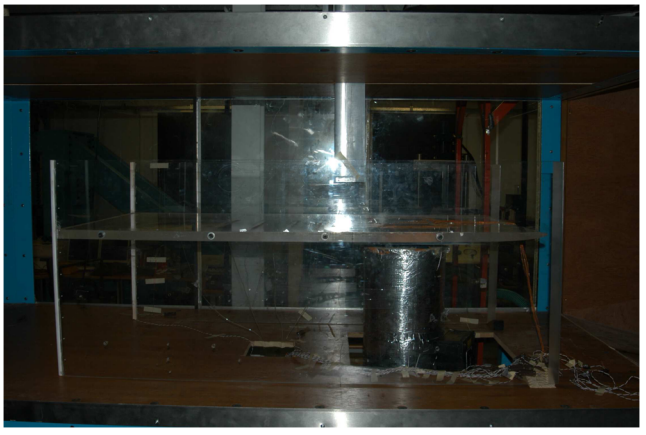

Fig. 6 Experimental setup.

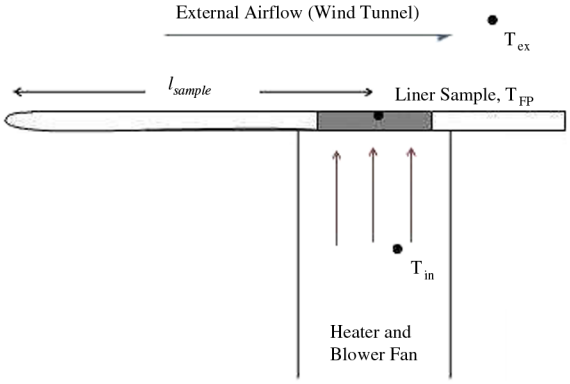

Fig. 7 Test apparatus.

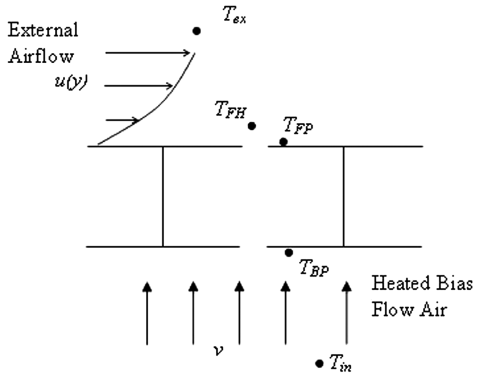

Fig. 9 Thermocouples positions in honeycomb cell.

approximately between 60 and 100°C. The maximum mass flow rate was 0.018 kgs^{-1}.

A pressure tapping was placed in the insulation layer (hatched layer in Fig. 8). This pressure tapping was used to measure the pressure just before the acoustic liner backing plate. A thermocouple was also placed in the open section at the insulation layer in order to measure the air temperature of the bias air flowing into the test sample.

3. *Instrumentation of Sample*

The sample was instrumented with T-type thermocouples. T-type thermocouples were chosen based on published literature for the same range of experimental testing conditions [24]. Thermocouples were placed at the outlets of five holes on the facing sheet, and T_{FH} represents the temperature measurement for the front holes. Five thermocouples were attached at equal spacing to both the facing T_{FP} and backing sheet, and T_{FP} represents the temperature measurement of front plate. The sample used a total of 15 thermocouples; see Fig. 9 for approximate positions of thermocouples.

4. *Measurements*

Thermocouples were connected to a National Instruments SCXI™, which was connected to a computer. LabVIEW™ software was used to analyze the data received from the thermocouples. Pressure measurements were made using a Furness Controls FCO510 digital manometer. The flow rate through the acoustic liner was measured using a Bailey Fischer and Porter 10VT1000 Vortex 4™ flowmeter.

The temperatures measured from the corresponding thermocouples were used to obtain the acoustic liner heat transfer coefficient. The acoustic liner heat transfer coefficient was calculated using the following equation:

$$h_{\text{liner}} = \frac{q_{\text{liner}}}{A_{\text{liner}}(T_{\text{in}} - T_{\text{FP}})} \tag{2}$$

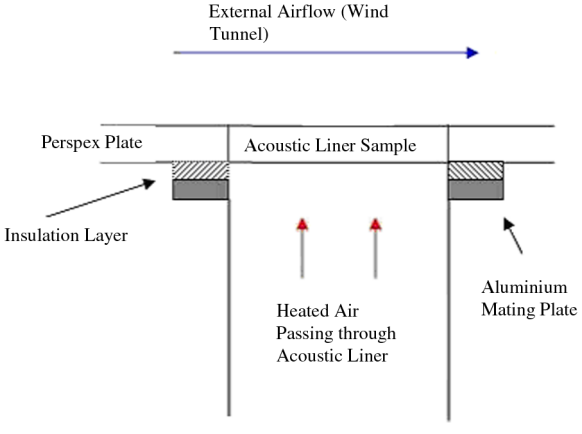

Fig. 8 Pressure tapings.

where h_{liner} is the overall heat transfer coefficient of the acoustic liner, q_{liner} is the heat loss across the acoustic liner, A_{liner} is the acoustic liner total area that is exposed to the exterior boundary layer, T_{FP} is the temperature of the front plate skin, and T_{in} is the temperature of the heated air.

The heat loss across acoustic liner q_{liner} is calculated using the following equation:

$$q_{\text{liner}} = \dot{m} c_p (T_{\text{in}} - T_{\text{FH}}) \tag{3}$$

where $\dot{m}$ is the mass flow of the heated air, c_p is the heat capacity of air at constant pressure, and T_{FH} is the temperature of the air exiting the holes on the front of the acoustic liner.

5. *Test Conditions*

The volume flow rates through the liner were varied from 0.2 to 1.1 $m^3\,min^{-1}$. Correspondingly, the voltage across the heater unit was varied between 100 to 150 V, along with varying the wind-tunnel speed between 10 and 30 ms^{-1}. The bias to grazing velocity ratio is between 0.015 and 0.077: that is for the bias velocity averaged over the entire front plate and not the hole exit bias velocity. This was all done in order to maximize the temperature difference between the liner top plate surface and the inlet air, so as to minimize error.

The thermocouple measurement error was estimated to be less than 5%. The manometer measurement error was estimated to be less than 2%. The flowmeter measurement error was estimated to be less than 2%.

B. Numerical Solution

An individual honeycomb cell in the acoustic liner was modeled as a three-dimensional grid. Providing there is no lateral conduction in the honeycomb [8], a single cell can be considered representative of the entire honeycomb. A modified grid was also created to investigate the effects of a burr on heat transfer and pressure loss across the acoustic liner. The numerical solution of the honeycomb cell was solved using a commercial computational fluid dynamics code, Fluent.

1. *Computational Domain*

Figure 10 shows the computational domain of the three-dimensional honeycomb cell. The computational domain is divided into three sections, with the honeycomb cell being the middle section. The honeycomb cell was constructed with the top surface having a large hole, of 9% open area of the total cross section area of the cell, while the bottom surface had a small hole, of 1% open area. The section before the small hole is the inlet section, and the section after the large hole is the outlet section.

Hexagonal geometry was used for the holes in the top and bottom plates (if their area is same as that of the equivalent circular holes, then the effects on flow can be neglected [14]).

The modified grid was effectively split into four sections. An extra section was inserted between the inlet section and the honeycomb

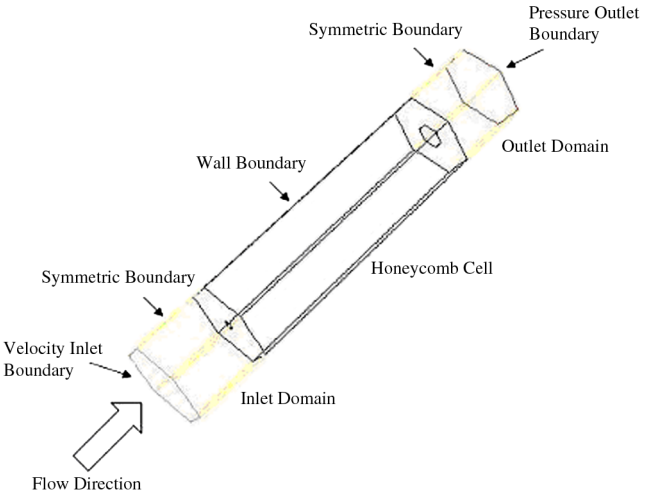

Fig. 10 Three-dimensional honeycomb cell.

cell to represent the plate thickness and the small duct of the back plate hole, as shown in Fig. 11.

Typical burr geometry was created at the exit of the back hole using typical values in available literature [25–27]; see Fig. 12. The geometry parameters used were burr radius of curvature to hole diameter ratio of 0.101 and chamfer length to hole diameter ratio of 0.1.

2. Boundary Conditions

Most of the boundary conditions were similar for all solutions of the honeycomb cell. The main differences in boundary conditions were those set at the honeycomb walls. The following is a list of all the boundary conditions:

1) A velocity inlet boundary condition was created at the beginning of the inlet for all grids; several cases were run for all grids in which the inlet velocity was varied from 0.2 to 0.9 ms^{-1}. The inlet flow direction was specified normal to the boundary. For all cases and grids, the inlet temperature was 343 K, the turbulence intensity was set at 5%, and the hydraulic diameter was set as the back hole diameter at 0.0007 m.

2) A pressure outlet boundary condition was set at the end of the outlet section for all grids and cases. Operating pressure was set to zero, so the gauge pressure was set to 101,325 Pa, and the backflow total temperature was set to 293 K; the backflow direction was specified normal to boundary. As with the velocity inlet, the turbulence intensity was set at 5% and the hydraulic diameter was set as the back hole diameter at 0.0007 m.

3) A symmetric boundary condition was set at the sides of the inlet and outlet sections.

4) The honeycomb cell top, side, and bottom surfaces were all set as a wall boundary condition with the properties of aluminum. Fluent's shell conduction model was enabled. The bias acoustic liner will typically have a grazing flow on its surface. The effect of the grazing flow will be to increase heat transfer between the liner surface and the freestream. However, the effect on the heat transfer mechanisms inside the honeycomb cell can be neglected [12]. To replicate this grazing flow, the top surface of the honeycomb cell had a negative heat generation rate of 8 $\mathrm{MW\ m}^{-3}$. This heat generation rate was calculated from the heat transfer coefficient for the turbulent boundary layer on a flat plate using a well-accepted expression [28].

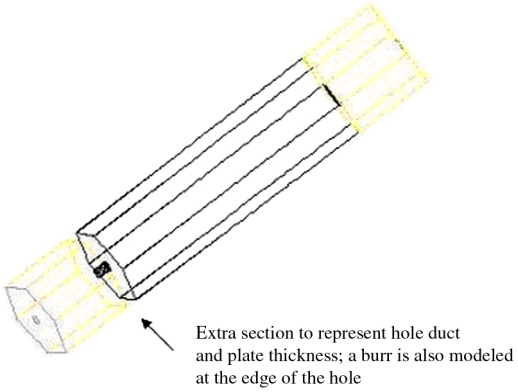

Fig. 11 Modified grid geometry.

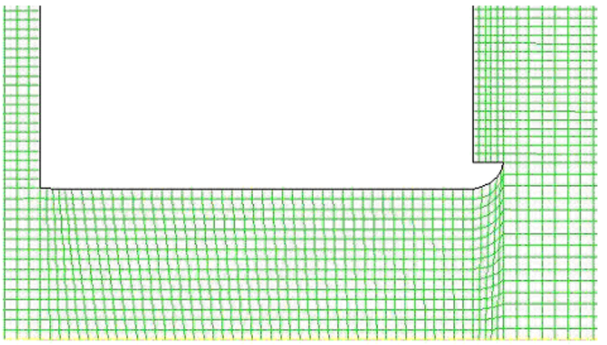

Fig. 12 Burr geometry.

5) For the modified grid, due to plate thickness being modeled, the two fluxes were placed on inlet and outlet sides of the bottom surface to model conduction through the back plate. Hence, a negative heat flux of 2 $\mathrm{kW\ m}^{-2}$ on the inlet side of the bottom surface and a positive flux of 2 $\mathrm{kW\ m}^{-2}$ was set on the outlet side of the bottom surface. The remaining surfaces within the hole and between the hole duct section and the honeycomb were set as wall boundaries with zero conduction properties.

3. Turbulence Model and Solver

A *k*-epsilon turbulence model with nonequilibrium wall functions was used for numerical solutions, because the *k*-epsilon model has been previously used to investigate turbulent jet structures [29–32]. In addition, to assess the choice of turbulent model, a number of other turbulent models, including the Reynolds stress model, were also used for a single case. The turbulent intensity was also varied; however, as can be seen from Figs. 13 and 14, turbulent model and turbulent intensity had minimal impact on the numerical solution. A second-order solver was used. A convergence criterion of 1×10^{-6} was used.

4. Grid Dependence

A grid dependency study was also carried out; see Figs. 15 and 16. Two meshes were created with 220,000 cells and 1,760,000 cells. The results of the numerical solution of each of the two meshes were compared. The maximum difference between the results from each mesh was found to be within 2%. The mesh with 220,000 cells was used.

III. Results and Discussion

A. Heat Transfer

Figure 17 shows the variation of both the acoustic liner and back plate Nusselt numbers $Nu_{A/P}$ against Reynolds numbers $Re_{A/P}$. The acoustic liner back plate was considered equivalent to a single porous plate, as the flow approaching the back plate is uniform and undisturbed. Therefore, Dorignac et al.'s experimental plate correlation [11] and the numerical solution for the back plate were included.

The Nusselt number and Reynolds number are defined as follows:

$$Nu_{A/P} = \frac{hA/P}{k_{\mathrm{air}}} \qquad Re_{A/P} = \frac{\rho V_{\mathrm{in}} A/P}{\mu}$$

where h is the heat transfer coefficient, A is the local active area around hole, P is the hole pitch, k_{air} is the conductivity of air, ρ is the

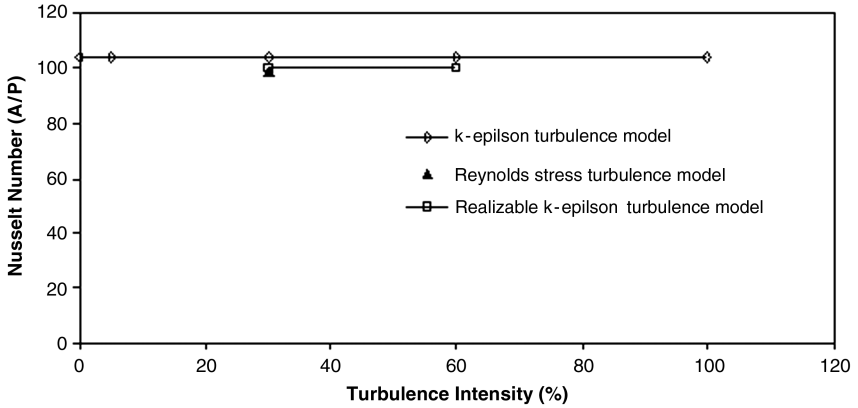

Fig. 13 Effect of turbulent models on heat transfer.

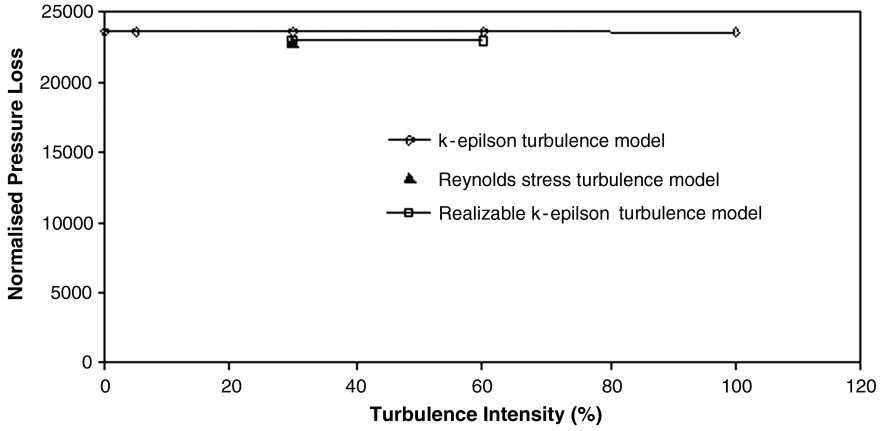

Fig. 14 Effect of turbulent models on pressure loss.

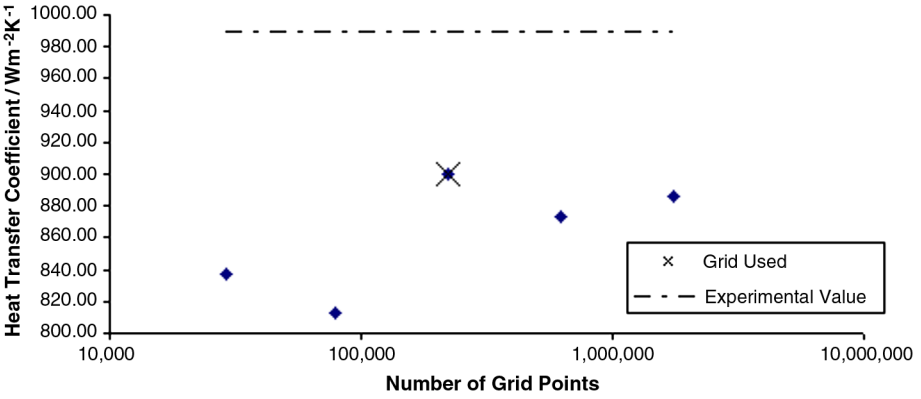

Fig. 15 Grid dependence study (heat transfer coefficient).

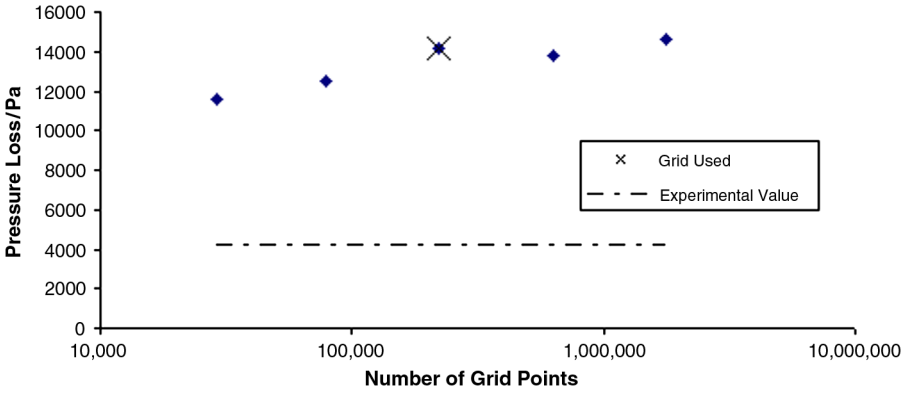

Fig. 16 Grid dependence study (pressure loss).

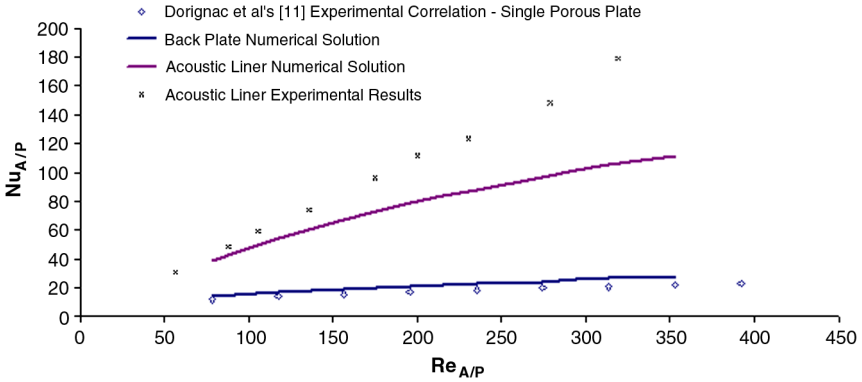

Fig. 17 Acoustic liner Nusselt number.

air density, V_{in} is the velocity downstream of the back porous plate, and μ is the dynamic viscosity of fluid.

Three-dimensional numerical and experimental results show that the acoustic liner has a higher heat transfer coefficient than the porous plate (or acoustic liner back plate). Although the difference between experimental and simulation results increases along with the increase of the Reynolds number, the results from the simplified single cell model compare well with the measurements at low Reynolds numbers and predict the increase trend of the Nusselt number with the increase of the Reynolds number.

The three-dimensional numerical solution for the back plate only slightly varies from Dorginac et al.'s experiment correlation [11]. When comparing the results for heat transfer across the entire acoustic liner to the front face, the three-dimensional numerical solution predicts a lower heat transfer coefficient, particularly at high flow rates. This is most likely due to the film cooling/heating effect of the heated air blowing into the freestream [33]. Experimental results for the entire acoustic liner show a steeper gradient than those of the three-dimensional numerical solution.

To fully understand the heat transfer mechanism of the bias liner, two approaches have been adopted with corresponding assumptions.

Initially, it was expected that there would be little or no heat transfer between the internal flow in the honeycomb cell and its sidewall. It was expected that heat would just be conducted from the back plate to the front plate, up along the sidewall. Based on these assumptions, a simple heat transfer model was derived using electric circuit analogy similar to that used by Wong et al. [22]. Therefore, the acoustic liner heat transfer coefficient could be calculated using Eq. (4):

$$h_{\text{Liner}} = \frac{h_{\text{HC}} h_{\text{BP}}(1-\sigma_{\text{BP}})}{h_{\text{HC}} + h_{\text{BP}}(1-\sigma_{\text{BP}})} + h_{\text{FP}}(1-\sigma_{\text{FP}}) \tag{4}$$

where h_{FP} is the front plate heat transfer coefficient, h_{BP} is the back plate heat transfer coefficient, σ_{FP} is front plate porosity, and σ_{BP} is the back plate porosity. The variable h_{HC} is an equivalent heat transfer coefficient for conduction defined as follows:

$$h_{\text{HC}} = \frac{k_e}{l} \tag{5}$$

where k_e is the effective conductivity, which was calculated using the Swann and Pitman model [5], and l is the length of the honeycomb cells. The acoustic liner back plate heat transfer coefficient can be calculated using Dorginac et al.'s correlation [11]. The front plate heat transfer coefficient can also be roughly estimated using Dorginac et al.'s correlation.

However, the results from both the three-dimensional numerical solution and the experiment give a higher heat transfer coefficient than that predicted by Eq. (4). Hence, the theory was modified assuming that the acoustic liner surface was isothermal and that the heat transfer between the internal honeycomb flow and the sidewalls was the same as that for fully developed duct flow, as shown in Eq. (6):

$$h_{\text{Liner}} = h_{\text{BP}}(1-\sigma_{\text{BP}}) + h_{\text{FD}}F + h_{\text{FP}}(1-\sigma_{\text{FP}}) \tag{6}$$

where h_{FD} is the heat transfer coefficient for fully developed duct flow, and F is a shape factor for the honeycomb wall defined as follows:

$$F = \frac{4l}{D} \tag{7}$$

where D is the hydraulic diameter of the honeycomb cells.

Both three-dimensional numerical and experimental results again give a higher heat transfer coefficient than that calculated using Eq. (6). A further literature search revealed that heat transfer between the internal honeycomb flow and the sidewalls can be five times that experienced in fully developed duct flow [20,21]. Peak heat transfer occurs at the point where the flow reattaches to the honeycomb

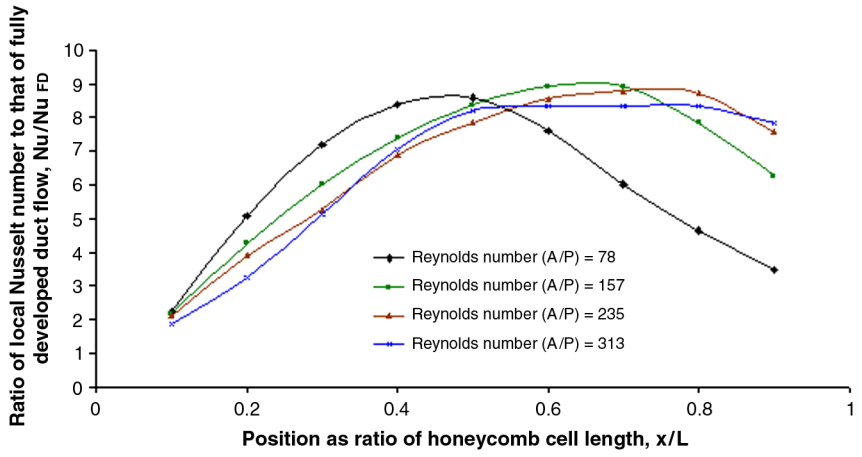

Fig. 18 Honeycomb sidewall transfer.

sidewall [20]. Actual values calculated from the three-dimensional numerical solution give values seven times that of fully developed duct flow; see Fig. 18. As the abrupt expansion ratio becomes larger, so do the sidewall heat transfer coefficients [20]. Figure 18 shows that the heat transfer is not uniform along the honeycomb cell wall, and the variation of heat transfer along the honeycomb cell wall also changes with Reynolds number. When the Reynolds number approaches 366, the heat transfer first increases with the increase of Reynolds number, then it tends to become uniform.

As a result, it has been seen through both the numerical solution and experiment results that the heat transfer coefficient of the acoustic liner is higher than that of the single porous plate.

This can be expected as the fluid passes through two porous plates rather than one. Two porous plates roughly double the active area where heat transfer between the fluid and the solid surface can take place. However, from Fig. 17, it can be seen that the heat transfer coefficient is more than double that of the back plate. Hence, it suggests that there are other effects present, such as heat transfer at the honeycomb sidewalls, as can be seen from Fig. 19. Moreover, this effect becomes stronger as the Reynolds number increases.

An additional numerical simulation was carried out. This time, it was just for one case with Fluent 's shell conduction feature turned off, but a heat flux was still placed on the front plate. Figure 20 shows the static temperatures for the shell conduction enabled. Figure 21 is the static temperature contours when shell conduction is disabled.

Comparing both figures shows that there are temperature gradients between the entire honeycomb cell surfaces and the internal fluid flow when shell conduction is enabled, whereas temperature gradients are only present at the front plate when the shell conduction is disabled. In summary, the numerical solution shows that heat transfer does occur between the honeycomb sidewalls and the internal fluid flow. All the flow inside in the honeycomb cell is turbulent at the start due to the separation as the flow exited the small back hole. Then, reattachment occurs, and finally, the flow will be forced laminar at the other end of the honeycomb cell as it impinges on the plate while exiting through the larger front hole.

Comparing Fig. 18 with that of Fig. 22 shows that the numerical solution roughly gives maximum heat transfer at the point of reattachment. These findings are supported in the previous research investigating heat transfer downstream of abrupt expansions [17,20]. The research work of Krall and Sparrow [17] and Baughn et al. [20,21] came to the following conclusions. In areas of recirculation just after the abrupt expansion or fully developed flow downstream of it, the local heat transfer coefficient was similar to that for fully developed duct flow. At points of reattachment, the heat transfer coefficient was found to peak reaching values between three to five

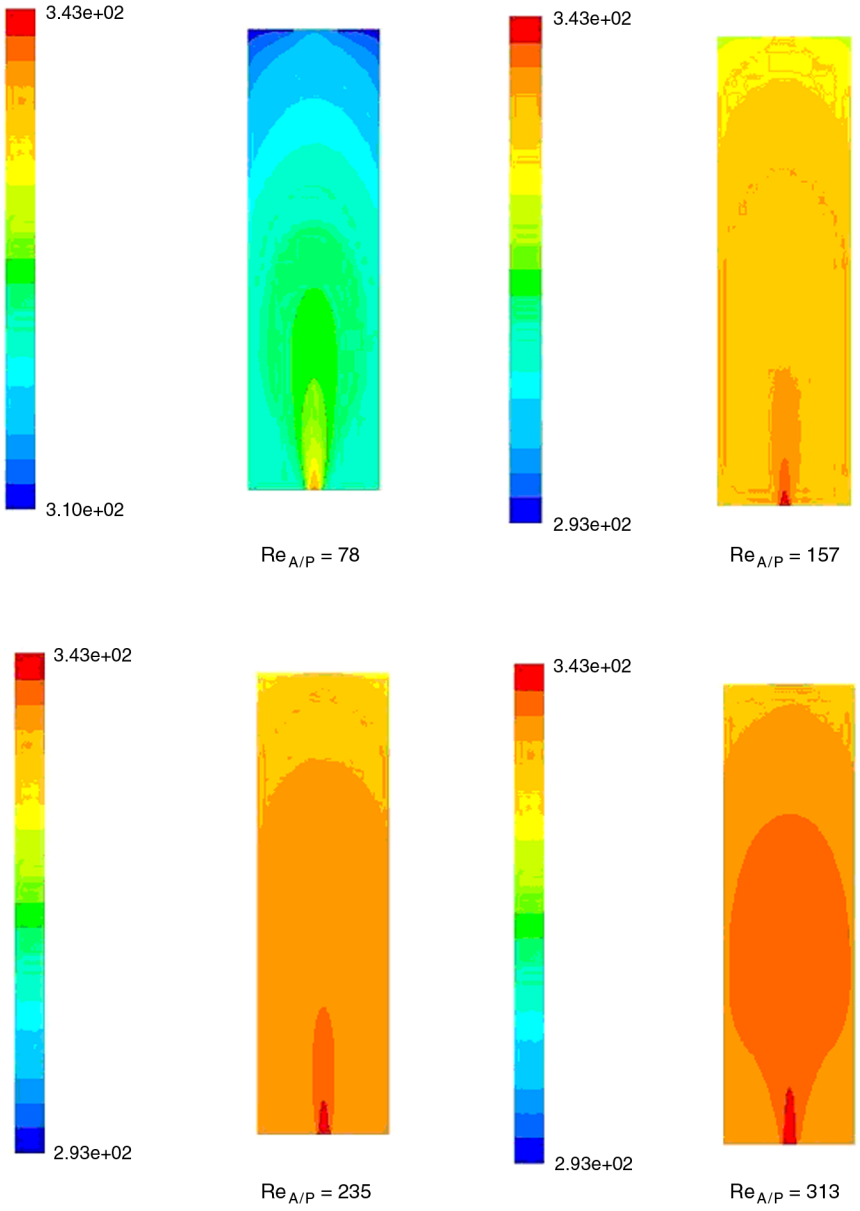

Fig. 19 Static temperature contours.

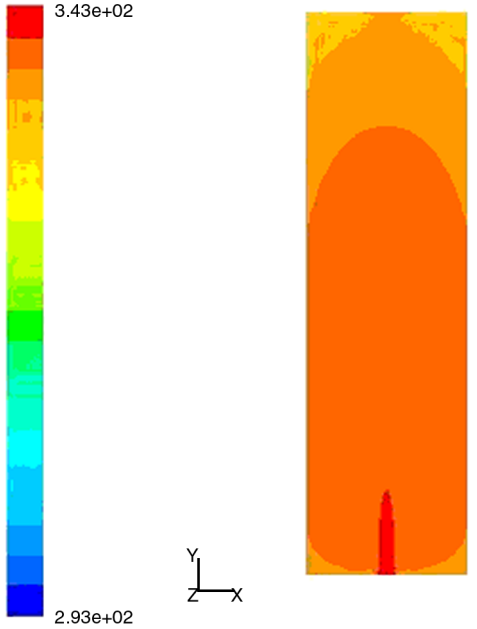

Fig. 20 Static temperature contours with shell conduction enabled ($Re_{A/P} = 353$).

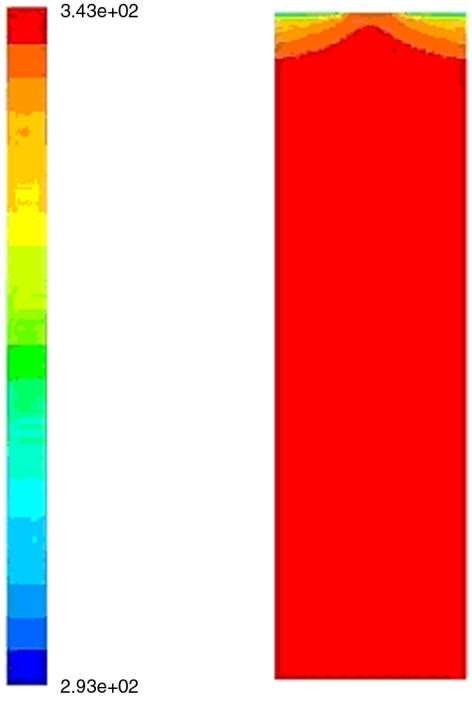

Fig. 21 Static temperature contours with shell conduction disabled ($Re_{A/P} = 353$).

times that found in fully developed duct flow. Other regions, such as those of developing flow, also had higher values of heat transfer coefficient: about twice that for fully developed flow. The point of reattachment moves up with the increase of the Reynolds number to a limit roughly one-third of the honeycomb length.

By turning the shell conduction off, heat transfer only occurs at the acoustic liner front plate, also making it possible to calculate the heat transfer coefficient of the front plate. It was found that the heat transfer coefficient of the front plate was within 27% of that calculated using Dorginac et al.'s experiment correlation [11]. It is believed that the large difference is due to the flow still having a small jet effect as it approaches the front plate. This is verified with Fig. 23, where only a small jet effect can be seen; this can be expected from the large depth to hole diameter ratio, $l/D = 31$.

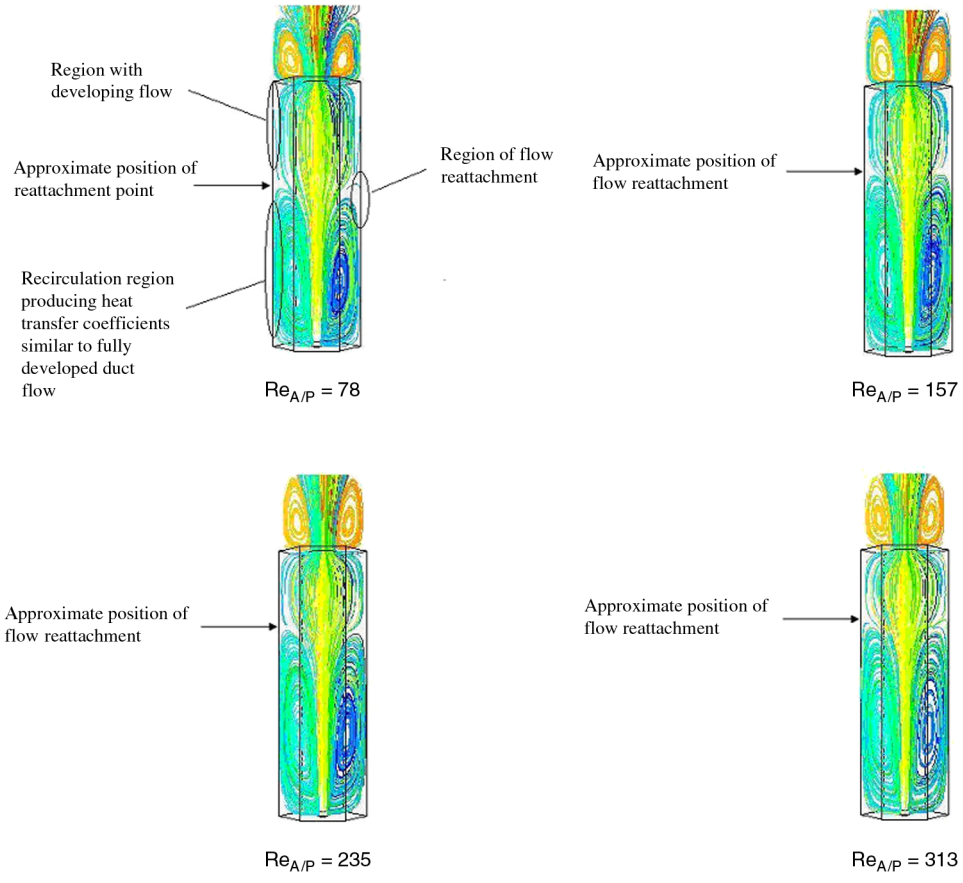

Fig. 22 Path lines.

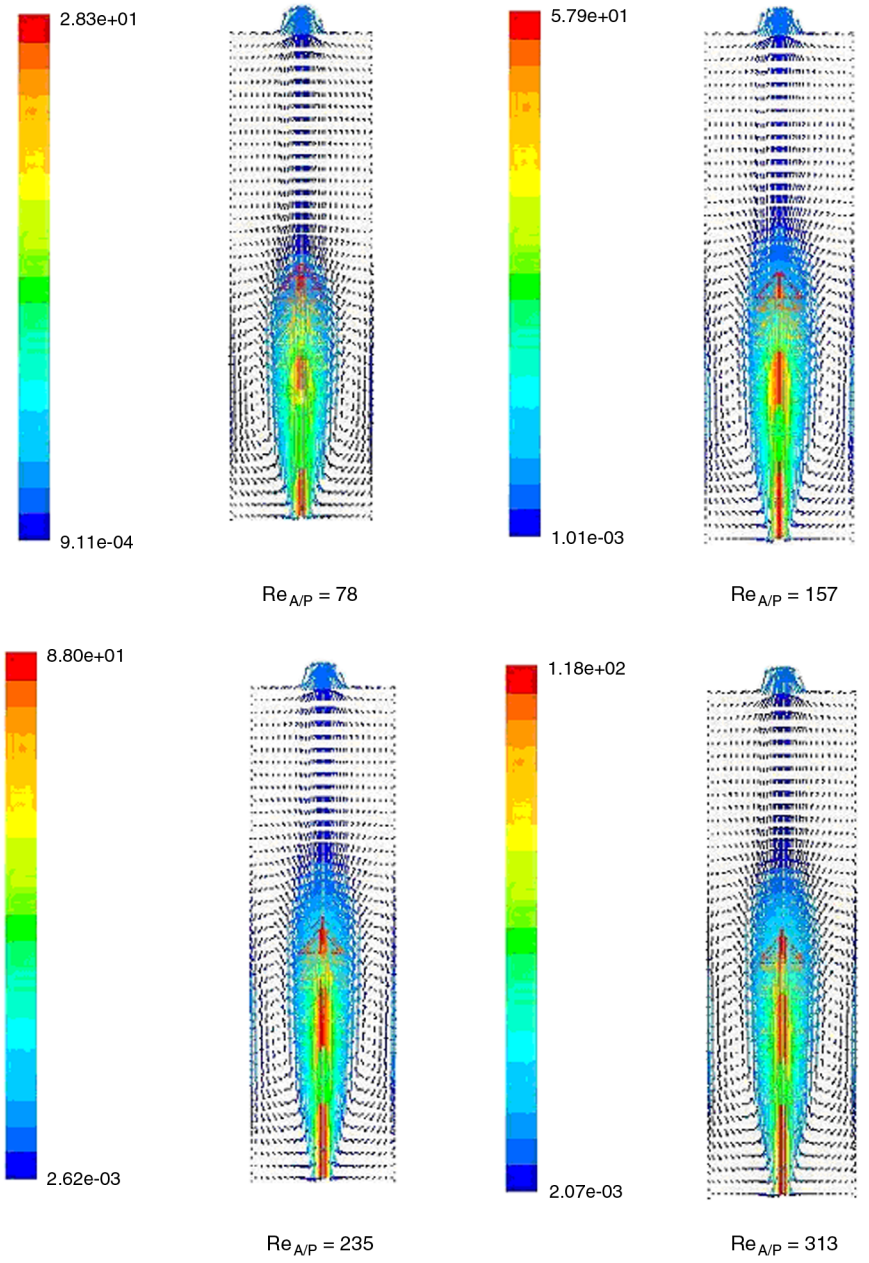

Fig. 23 Velocity vectors.

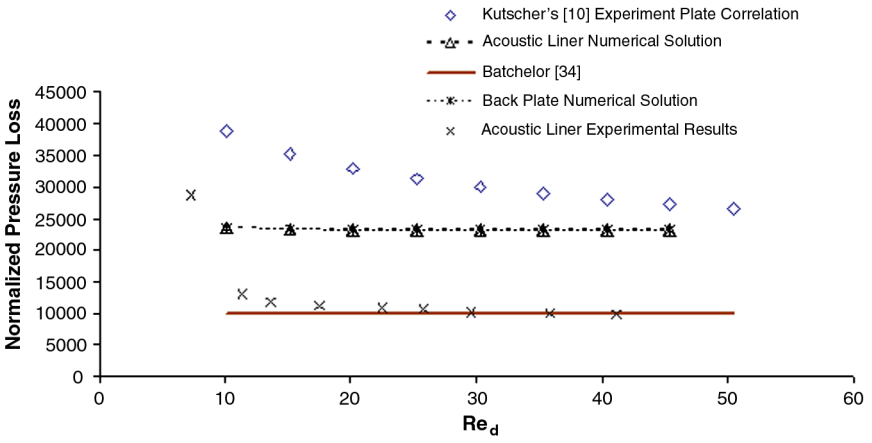

Fig. 24 Acoustic liner normalized pressure loss.

A percentage of 17.6 of the total heat transfer occurs at the front plate. A percentage of 14.7 of the total heat transfer occurs at the back plate. The remaining heat transfer occurs at the honeycomb sidewalls.

B. Pressure Loss

Figure 24 shows that the normalized pressure loss across the acoustic liner back plate is the most significant, as can be expected due to the small size of holes in the back plate compared with those in the front plate. Therefore, the pressure losses across the front plate can be neglected.

For pressure loss, the numerical solution for back plate only varies slightly with that of Kutscher's experimental correlation [10]. However, experimental results for an acoustic liner show a lower pressure loss agreeing with the traditional expression for pressure loss across abrupt expansions and porous plates [34]. As the Reynolds number is further reduced, the flow does tend toward Kutscher's experimental correlation [10].

Normalized pressure and Reynolds number are defined as follows:

$$\zeta = \frac{\Delta p}{(1/2)\rho V_{\text{up}}^2} \qquad Re_d = \frac{\rho V_{\text{up}} d}{\mu}$$

where ζ is normalized pressure, Δp is pressure loss, and d is back plate hole diameter.

The difference between experimental results and the numerical solution was left unexplained in a previous publication [35]. Kutscher's experimental findings concluded that a dependence on Reynolds number for porous plates with small hole diameters was the result of strong viscous losses in the holes [10]. He said these viscous losses were the result of forced laminar flow in the small holes.

Therefore, it was thought that the difference between the experiment results and the numerical solution could be caused by large turbulence effects in the experiment setup, as the bias flow air was provided by a blower fan, which then passed through a series of heating elements. This was very likely to cause high levels of turbulence. Higher levels of turbulence in the bias flow may have prevented forced laminar flow in the holes of the porous plate, hence giving a lower pressure loss.

Further numerical work was carried out to determine if this was the case. The numerical solution was improved by refining the mesh; cell density was increased within and close to the back plate holes. Turbulence intensity was varied in the numerical solution to see if it had any effect on normalized pressure loss. Turbulence models, wall functions, etc. were all varied to see if they had any effect on pressure loss. However, these all proved to have only a small effect on the pressure loss: about a 5% change.

At this point, it was decided to modify the numerical model to investigate the effects of the back hole geometry on pressure loss.

C. Modified Numerical Solutions

First, a very simple mesh was created just to simulate the back plate of the acoustic liner. With attention focusing on the geometry of the back plate holes, the first major difference that had been overlooked was the plate thickness relative to the hole diameter.

The plate thickness was 1 mm, while the hole diameter was 0.7 mm; the original numerical solution had modeled a plate of negligible thickness compared with hole diameter, so the grid was modified to take account of plate thickness. Various simulations were carried out for plates of different thicknesses. However, from Fig. 25, it can be seen that the lowest pressure loss was for a plate thickness ratio of about 0.8. For the test samples geometry, the normalized pressure loss was about 19,391, still about twice the value of the experimental results that give about 9801.

The further reduction in pressure loss was thought to be caused by the presence of a burr at the outlet of the back hole. Two geometry parameters were considered to have an effect on pressure loss, the length of the burr L_0, and the radius of the curvature of the burr R_0. The effects of these geometry parameters are displayed in Figs. 26 and 27.

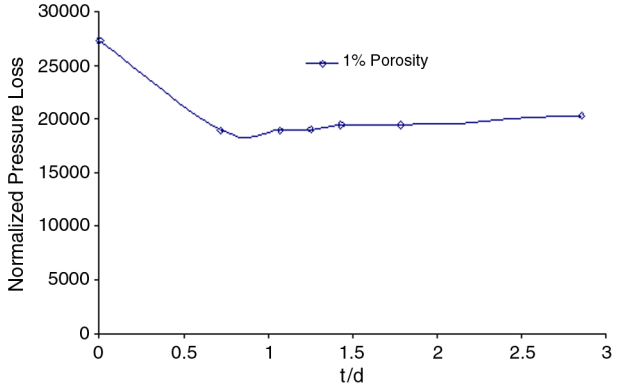

Fig. 25 Normalized pressure loss against t/d.

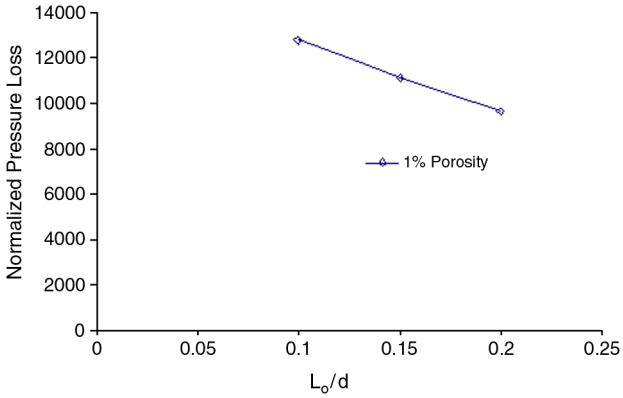

Fig. 26 Normalized pressure loss against L_o/d.

More realistic values of burr geometry based on published work [25] (that is, $L_o/d = 0.1$ and $R_o/d = 0.101$) were chosen, which gave a normalized pressure loss of 15,217. A simulation of the honeycomb cell with a burr at the back hole was carried out to see what effects hole geometry had on heat transfer characteristics. This simulation was compared with a grid without a burr at the back plate. This solution was also compared with the experimental results; see Fig. 28. As shown in Fig. 28, the simulation results (shown by a dashed line) are still about 64% higher than the normalized pressure loss given by experimental results (shown by ×); however, the results are not only closer to the experimental results, but they also show the dependency of the pressure loss on the Reynolds number with the same trend. The numerical results for the larger back plate porosity were also included. By comparing these three sets of results, acoustic liner experimental data, acoustic liner numerical solution of 1% back plate porosity (modified grid), and 3% back plate porosity, it is reasonable to conclude that the viscous losses (i.e., forced laminar flow in small holes) are one of the factors affecting pressure loss. This

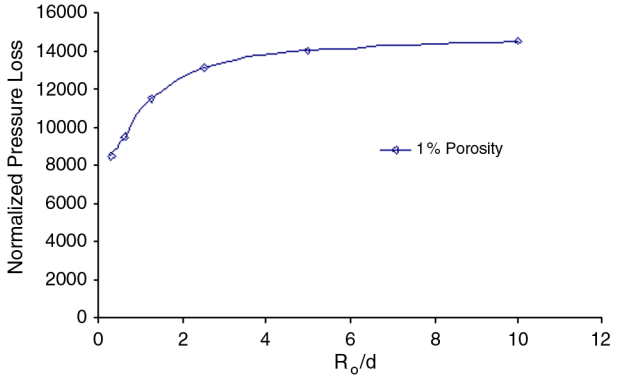

Fig. 27 Normalized pressure loss against R_o/d.

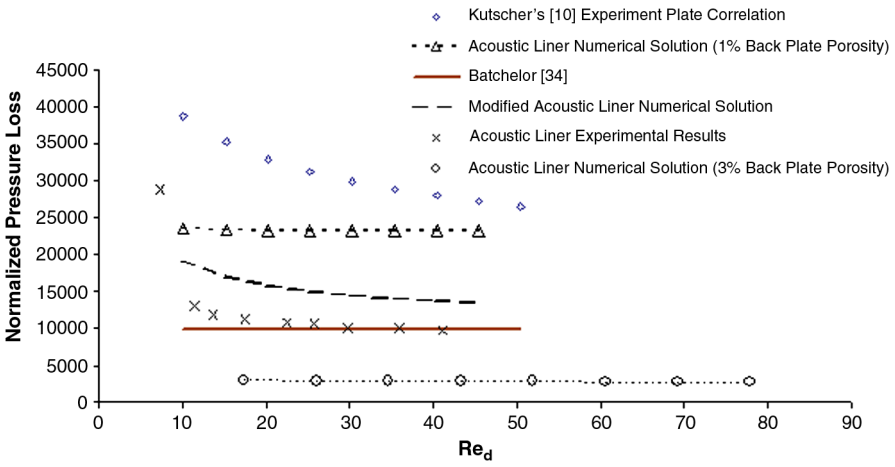

Fig. 28 Comparison of acoustic liner with burr.

demonstrates that hole geometry has a significant effect on pressure loss that is also supported by Broach et al.'s findings [16].

The work by Kutscher [10] suggested that relaminarization would occur in the holes for the experiment; hence, there would be a high pressure loss. However, as the initial numerical solution was completed before the experiment, the results of that solution were expected to correspond to that of Batchelor [34]; the traditional expression assuming relaminarization does not occur in the holes. But the initial numerical solution agreed more closely with Kutscher [10], suggesting that, in Fluent, the *K*-epsilon turbulence model could detect relaminarization. Once the experiment was completed, the result gave a lower pressure loss, agreeing almost perfectly with Batchelor [34], suggesting that, in practice (for this specific case), relaminarization did not occur. Therefore, increases in turbulence intensity and various other turbulence models (including the Reynolds stress model) were tried for one case, but this produced no significant effect on pressure loss. Only when the hole geometry was modified was the pressure loss significantly affected. This concludes that the hole geometry (or defect, mainly burr and plate thickness) was preventing the flow relaminarizing in the holes. This is supported by Broach et al. [16], who experimentally demonstrated that changes in hole geometry can significantly effect pressure loss values, and it is particularly important in some applications where plate porosity, etc. cannot be modified.

Figure 29 gives the graph of a Nusselt number plotted against a Reynolds number, comparing different numerical results with the

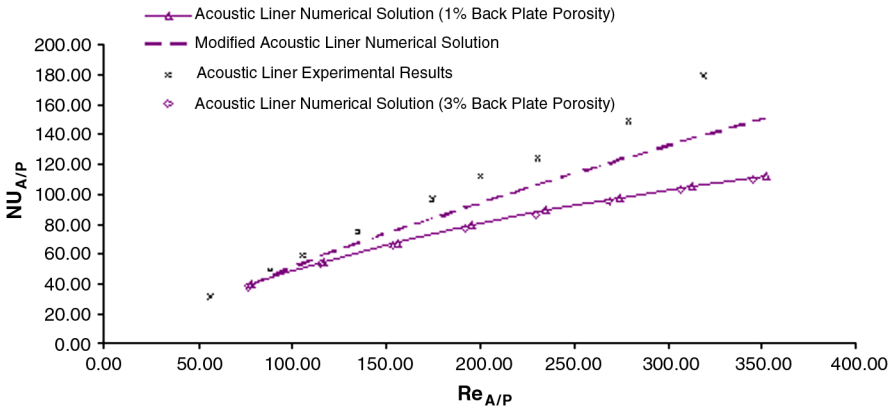

Fig. 29 Effects of burr on heat transfer.

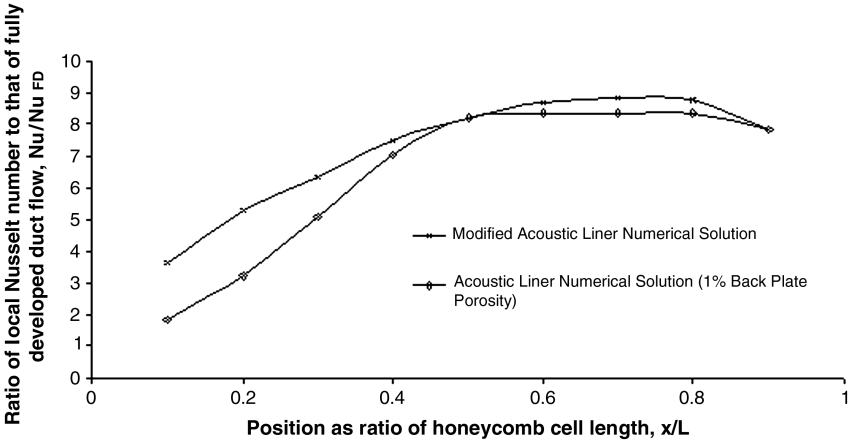

Fig. 30 Comparison of sidewall heat transfer ($Re_{A/P} = 313$).

experimental results. The numerical solution of the cell with modified geometry gives higher heat transfer than that of the original model, which is closer to that of the experimental results. Furthermore, the modified solution also shows a steeper gradient toward the experimental results. These findings show that small irregularities not modeled in numerical models can produce differences between the numerical solution and experimental results. This again was thought to be due to geometry effects of the hole, as Fig. 29 shows that the geometry defects also affect heat transfer as well as pressure loss. The reason for the higher heat transfer close to the back plate and flow reattachment point is most likely due to the burr reducing the amount of energy extracted from the jet, hence allowing it to attach to the wall more gradually and at a greater speed. The numerical results for the larger back hole give the same heat transfer as the numerical results for original back hole size, i.e., the smaller hole size. The maximum difference between experimental and numerical results for the modified solution is 16% compared with 37% for the original solution.

Figure 30 shows the ratio of the local sidewall Nusselt number to equivalent fully developed duct flow The Nusselt is number plotted against the sidewall position at the same Reynolds number. The graph compares the original numerical solution to the modified numerical solution. The modified numerical solution predicts higher heat transfer in regions close to the back plate and at the flow reattachment point. The reason for the higher heat transfer close to the back plate and flow reattachment point is most likely due to the burr reducing the amount of energy extracted from the jet, hence allowing it to attach to the wall more gradually and at a greater speed.

IV. Conclusions

The numerical solution for the acoustic liner back plate Nusselt number varies only slightly from that of Dorignac et al.'s experiment correlation [11]. A higher heat transfer rate than expected is achieved for the acoustic liner that is verified by both numerical solution and experiment. The primary reason for this is an increase in heat transfer in the region where the flow inside each of the honeycomb cells reattaches to the sidewalls after exiting a small hole.

Initially, the simulation of the simplified model does not match with the experimental results for pressure loss due to idealization or ignorance of the difference in the hole geometry. Experimental results for normalized pressure loss were found to agree with the traditional expression for pressure loss across abrupt expansions and porous plates [34]. The numerical solution agreed with Kutscher's experiment correlation [10]. Further literature review revealed that hole outlet geometry has a significant effect on heat transfer and pressure loss characteristics [16]. Therefore, a modified model was developed, and the solution was improved. It was found that the presence of a burr at the hole outlet gave better agreement with experimental results.

Appendix A: Energy Balance at each Acoustic Liner Component

The overall heat transfer coefficient of the acoustic liner h_{Liner} is defined as follows:

$$\dot{q}_{\text{Liner}} = h_{\text{Liner}} A_T (T_{\text{in}} - T_{\text{FP}}) \tag{A1}$$

where $\dot{q}_{\text{Liner}}$ is total heat transfer rate through the acoustic liner, A is the total facing sheet area of the acoustic liner, T_{in} is the temperature of the heated bleed air, and T_{FP} is the temperature of the front plate skin. The liner heat transfer coefficient will mainly be a function of the acoustic liner plate and honeycomb geometry, as well as the flow rates. The heat transfer coefficient of the grazing boundary layer is defined as follows:

$$\dot{q}_{\text{BL}} = h_{\text{BL}} A_T (T_{\text{FP}} - T_{\infty}) \tag{A2}$$

where $\dot{q}_{\text{BL}}$ is the heat swept away by the grazing boundary layer, and T_{∞} is the temperature of the freestream. Both the heat transfer coefficients of the grazing flow boundary layer and the acoustic liner use the total area of the liner facing sheet A_T as their reference area. Assuming that the total heat transfer through the acoustic liner is swept away by the grazing boundary layer, then

$$\dot{q}_{\text{Liner}} = \dot{q}_{\text{BL}}$$

In other words, the total heat passed through the liner is then passed into the grazing flow boundary layer. In calculating the overall heat transfer coefficient of a complicated system where there is a number of heat transfer coefficients involved, an electric circuit analogy is useful. This makes it simpler to visualize the problem and combine various heat transfer coefficients:

$$\Delta T = \frac{1}{h}\frac{\dot{q}}{A_T} \qquad V = R_E I$$

Comparing the equation for the heat transfer rate with that for electric current, it can be seen that the potential difference V is the analogy of the temperature difference ΔT. Electrical resistance R_E is the analogy of the inverse heat transfer coefficient $1/h$. The electrical current I is the analogy of heat flux $\dot{q}/A_T$. Starting with the heat transfer between bias flow fluid and the back plate skin, the back plate heat transfer coefficient h_{BP} is defined by the following equation:

$$\dot{q}_{\text{BP}} = h_{\text{BP}} A_T (1 - \sigma_{\text{BP}})(T_{\text{in}} - T_{\text{BP}}) \tag{A3}$$

where $\dot{q}_{\text{BP}}$ is the heat transfer rate between the bias flow fluid and the back plate skin, σ_{BP} is the back plate porosity, and T_{BP} is the temperature of back plate skin. Assuming that the heat transferred into the back plate is then conducted away by the honeycomb walls, and neglecting effects of the jet sweeping the sidewalls, etc., then

$$\dot{q}_{\text{BP}} = \dot{q}_{\text{Cond}} = h_{\text{HC}} A_T (T_{\text{BP}} - T_{\text{FP}}) \tag{A4}$$

where h_{HC} is the conduction heat transfer coefficient, which was defined in Eq. (5), k_e is an effective conductivity, and L is the length of the honeycomb cells. If the heat transfer to the honeycomb walls by other effects, such as free jet reattachment and vortices, etc., is assumed to be negligible, then it can be said that heat transfer conducted through the honeycomb walls and back plate skin are equal. Hence, the heat transfers happen one after another; therefore, an analogy can be made with two resistors connected in series; see Fig. A1:

From circuit analysis, combining resistors in series is simply

$$R_T = R_1 + R_2 + R_3 + \cdots\cdots + R_i$$

This is applicable to inverse heat transfer coefficients, so from Fig. A1,

$$\frac{1}{h_1} = \frac{1}{h_{\text{BP}}(1 - \sigma_{\text{BP}})} + \frac{1}{h_{\text{HC}}}$$

Rearranging gives the combined heat transfer coefficient for the whole system h_1:

$$h_1 = \frac{h_{\text{HC}} h_{\text{BP}} (1 - \sigma_{\text{BP}})}{h_{\text{HC}} + h_{\text{BP}}(1 - \sigma_{\text{BP}})}$$

The bias flow fluid will emerge from the back plate hole as a jet and impinge on the front plate. As already stated, impingement of the free jet on the front plate skin will transfer some heat into the skin. The heat transfer coefficient between the free jet and the front plate skin h_{imp} is defined as

$$\dot{q}_{\text{imp}} = h_{\text{imp}} A_T (1 - \sigma_{\text{FP}})(T_{\text{BH}} - T_{\text{FP}}) \tag{A5}$$

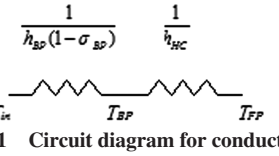

Fig. A1 Circuit diagram for conduction.

where $\dot{q}_{\text{imp}}$ is the energy transferred from the free jet at the back plate hole to the front plate skin, σ_{FP} is the porosity of the front plate skin, and T_{BH} is the temperature in the back plate hole. However, a more useful heat transfer coefficient is that between the heated bleed air and the front plate skin, as follows:

$$\dot{q}_{\text{imp}} = h_{\text{FP}} A_T (1 - \sigma_{\text{FP}})(T_{\text{in}} - T_{\text{FP}}) \tag{A6}$$

As can be seen from the preceding equation, the heat transfer rate is the same with the exception of temperature difference. Variables h_{FP} and h_{imp} are related by the following equation; see Appendix B for an full explanation:

$$h_{\text{FP}} = h_{\text{imp}} \left(1 - \frac{h_1 A_T}{\dot{m} c_p} \right) \tag{A7}$$

where $\dot{m}$ is mass flow of the bias flow, and c_p is the heat capacity of the fluid at constant pressure. Most analytic methods for heat transfer of free jets impinging on a surface are in the form of Eq. (A5). When using the circuit analogy to find the total heat transfer coefficient of the acoustic liner, it must be in the form of Eq. (A6).

Figure A2 shows a complete circuit diagram for the acoustic liner. The heat transferred through impingement of the free jet on the front plate takes a different path from the heat transferred by conduction. The temperature difference for impingement is the same as that for conduction. This is the same behavior as resistors in parallel. From circuit analysis to combine resistors in parallel is simply

$$\frac{1}{R_T} = \frac{1}{R_1} + \frac{1}{R_2} + \frac{1}{R_3} + \cdots\cdots + \frac{1}{R_i}$$

Hence, the same applies to Fig. A2:

$$h_{\text{Liner}} = \frac{1}{(1/h_{\text{HC}}) + \{1/[h_{\text{BP}}(1 - \sigma_{\text{BP}})]\}} + h_{\text{FP}}(1 - \sigma_{\text{FP}})$$

Rearranging the preceding equation gives the combined heat transfer coefficient for the whole system h_{Liner}, which is defined in Eq. (4). As the jet reattaches or sweeps the honeycomb sidewalls, it gives a heat transfer rate at the point of attachment that is five to seven times that of the fully developed pipe flow at an equivalent Reynolds number. A simple expression for the overall acoustic liner heat transfer coefficient can be derived from a circuit analogy, as in the previous section. The circuit can be simplified by assuming that temperatures remain equal and constant on the front plate, back plate, and honeycomb sidewalls. Hence, the acoustic liner is assumed to be isothermal and have perfect conduction, and the circuit diagram for this case is given in Fig. A3.

Figure A3 assumes perfect conduction, hence all heat transfer coefficients are due to forced convection heat transfer from the bias flow fluid to the back plate, front plate, and honeycomb sidewalls. The total heat transfer coefficient for the isothermal acoustic liner with perfect conduction can be derived from the circuit diagram and gives Eq. (6), where h_{Swept} is the average heat transfer coefficient for the sweeping jet flow, F is a shape factor for the honeycomb wall

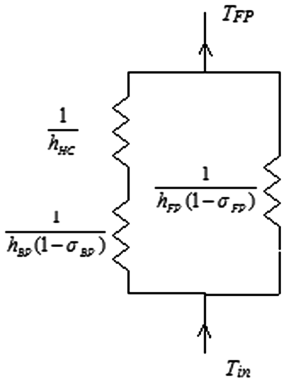

Fig. A2 Circuit diagram for acoustic liner.

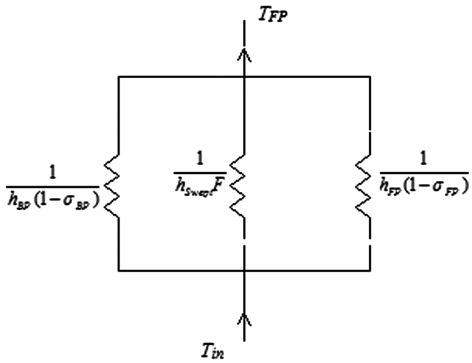

Fig. A3 Circuit diagram for sweeping.

defined in Eq. (7), and D is the hydraulic diameter of the honeycomb cells. Most of the heat transfer coefficients in Eq. (7) can be calculated. If the peak heat transfer and the distribution of the heat transfer are known, an average heat transfer coefficient can be determined for the sweeping flow on the sidewalls. The front plate heat transfer coefficient can be found using Eq. (A7).

Appendix B: Acoustic Liner Impingement Heat Transfer

The heat rate transferred between the back plate hole and the front plate skin through impingement of the jet on the front plate is given by Eq. (A5). However it would be useful to get a heat transfer coefficient in terms of the temperature difference $(T_{\text{in}} - T_{\text{FP}})$, as in Eq. (A6). The heat conducted through the honeycomb walls is given as follows:

$$\dot{q}_{\text{BP}} = \dot{q}_{\text{HC}} = h_1 A_T (T_{\text{in}} - T_{\text{FP}}) \tag{B1}$$

where

$$h_1 = \frac{h_{\text{HC}} h_{\text{BP}} (1 - \sigma_{\text{BP}})}{h_{\text{HC}} + h_{\text{BP}}(1 - \sigma_{\text{BP}})} \tag{B2}$$

Assuming that the heat lost between the box section and the back plate hole is conducted away through the honeycomb walls,

$$\text{energy in} = \dot{m} c_p T_{\text{in}} \qquad \text{energy out} = \dot{m} c_p T_{\text{BH}} + \dot{q}_{\text{BP}}$$

If energy is conserved.

$$\text{energy in} = \text{energy out}$$

Therefore,

$$\dot{m} c_p T_{\text{in}} = \dot{m} c_p T_{\text{BH}} + \dot{q}_{\text{BP}} \tag{B3}$$

Rearranging

$$T_{\text{BH}} = T_{\text{in}} - \frac{\dot{q}_{\text{BP}}}{\dot{m} c_p} \tag{B4}$$

Substituting Eq. (B1) into Eq. (B4) gives

$$T_{\text{BH}} = T_{\text{in}} - \frac{h_1 A_T (T_{\text{in}} - T_{\text{FP}})}{\dot{m} c_p} \tag{B5}$$

Substituting Eq. (B5) into Eq. (A5) gives

$$\dot{q}_{\text{imp}} = h_{\text{imp}} A_T (1 - \sigma_{\text{FP}}) \left(T_{\text{in}} - \frac{h_1 A_T (T_{\text{in}} - T_{\text{FP}})}{\dot{m} c_p} - T_{\text{FP}} \right)$$

Expanding gives

$$\dot{q}_{\text{imp}} = h_{\text{imp}} A_T (1 - \sigma_{\text{FP}})(T_{\text{in}} - T_{\text{FP}}) - \frac{h_{\text{imp}} h_1 A_T^2 (1 - \sigma_{\text{FP}})(T_{\text{in}} - T_{\text{FP}})}{\dot{m} c_p}$$

Tidying up gives

$$\dot{q}_{\text{imp}} = h_{\text{imp}} A_T (1 - \sigma_{\text{FP}}) \left(1 - \frac{h_1 A_T}{\dot{m} c_p}\right) (T_{\text{in}} - T_{\text{FP}}) \qquad \text{(B6)}$$

Comparing Eqs. (A6) and (B6) shows how h_{FP} can be related to h_{imp}, as in Eq. (A7).

References

[1] Dean, P. D., and Tester, B. J., "Duct Wall Impedance Control as an Advanced Concept for Acoustic Suppression," NASA CR-134998, 1975.

[2] Sun, X., Jing, X., and Zhang, H., "Effect of Grazing-Bias Flow Interaction on Acoustic Impedance of Perforated Plates," *Journal of Sound and Vibration*, Vol. 254, No. 3, 2002, pp. 557–573. doi:10.1006/jsvi.2001.4110

[3] Eldredge, J. D., and Dowling, A. P., "The Absorption of Axial Acoustic Waves by a Perforated Liner with Bias Flow," *Journal of Fluid Mechanics*, Vol. 485, No. 485, 2003, pp. 307–335. doi:10.1017/S0022112003004518

[4] Rademaker, E. R., and Demmenie, E. A., "The Development of an In-Situ Impedance Measurements on Air-Injected Acoustic Liners," *33rd International Congress and Exposition on Noise Control Engineering, Inter-Noise*, Czech Republic, International Inst. of Noise Control, New York, 2004, pp. 1–8.

[5] Swann, R. T., and Pitman, C. M., "Analysis of Effective Thermal Conductivities of Honeycomb-Core and Corrugated-Core Sandwich Panels," NASA TN D-714, 1961.

[6] Daryabeigi, K., "Heat Transfer in Adhesively Bonded Honeycomb Core Panels," *Journal of Thermophysics and Heat Transfer*, Vol. 16, No. 2, 2002, pp. 217–221. doi:10.2514/2.6687

[7] Lu, T. J., "Heat Transfer Efficiency of Metal Honeycombs," *International Journal of Heat and Mass Transfer*, Vol. 42, No. 11, 1999, pp. 2031–2040. doi:10.1016/S0017-9310(98)00306-8

[8] Asako, Y., Yamaguchi, Y., and Yamanaka, T., "Unsteady Three-Dimensional Natural Convection in an Inclined Air Slot with a Hexagonal Honeycomb Core," *29th National Heat Transfer Conference*, Vol. 237, Atlanta, GA, American Soc. of Mechanical Engineers, Fairfield, NJ, 1993, pp. 21–27.

[9] Sparrow, E. M., and Ortiz, M. C., "Heat Transfer Coefficients for the Upstream Face of a Perforated Plate Positioned Normal to an Oncoming Flow," *International Journal of Heat and Mass Transfer*, Vol. 25, No. 1, 1982, pp. 127–135. doi:10.1016/0017-9310(82)90241-1

[10] Kutscher, C. F., "Heat Exchange Effectiveness and Pressure Drop for Air Flow Through Perforated Plates with and Without Crosswind," *Journal of Heat Transfer*, Vol. 116, No. 2, 1994, pp. 391–399. doi:10.1115/1.2911411

[11] Dorignac, E., Vullierme, J., and Broussely, M., "Experimental Heat Transfer on the Windward Surface of a Perforated Flat Plate," *International Journal of Thermal Sciences*, Vol. 44, No. 9, 2005, pp. 885–893. doi:10.1016/j.ijthermalsci.2004.11.012

[12] Cho, H. H., and Goldstein, R. J., "Heat (Mass) Transfer and Film Cooling Effectiveness with Injection Through Discrete Holes. Part I: Within Holes and on the Back Surface," *Proceedings of the ASME Winter Conference*, New Orleans, LA, American Soc. of Mechanical Engineers, Fairfield, NJ, 1993, pp. 1–11.

[13] Cho, H. H., Jabbari, M. Y., and Goldstein, R. J., "Experimental Mass (Heat) Transfer in and Near a Circular Hole in a Flat Plate," *International Journal of Heat and Mass Transfer*, Vol. 40, No. 10, 1997, pp. 2431–2443. doi:10.1016/S0017-9310(96)00270-0

[14] Gan, G., and Riffat, S. B., "Pressure Loss Characteristics of Orifice and Perforated Plates," *Experimental Thermal and Fluid Science*, Vol. 14, No. 2, 1997, pp. 160–165. doi:10.1016/S0894-1777(96)00041-6

[15] Marjanovic, P., and Djordjevic, V., "On the Compressible Flow Losses Through Abrupt Enlargements and Contractions," *Journal of Fluids Engineering*, Vol. 116, No. 4, 1994, pp. 756–762. doi:10.1115/1.2911846

[16] Broach, K. D., Norrell, J. L., and Conner, M. E., "Perforated Plate Pressure Losses with Improved Inlet and Outlet Flow Hole Features," *4th ASME/JSME Joint Fluids Engineering Conference*, Vol. 1 B, Honolulu, HI, American Soc. of Mechanical Engineers, Fairfield, NJ, 2003, pp. 767–772.

[17] Krall, K. M., and Sparrow, E. M., "Turbulent Heat Transfer in Separated, Reattached, and Redevelopment Regions of Circular Tube," *Journal of Heat Transfer*, Vol. 88, No. 1, 1966, pp. 131–136.

[18] Zemanick, P. P., and Dougall, R. S., "Local Heat Transfer Downstream of Abrupt Circular Channel Expansion," *Journal of Heat Transfer*, Vol. 92, No. 1, 1970, pp. 53–60. doi:10.1115/1.3449645

[19] Amano, R. S., "Study of Turbulent Flow Downstream of an Abrupt Pipe Expansion," *AIAA Journal*, Vol. 21, No. 10, 1983, pp. 1400–1405. doi:10.2514/3.8259

[20] Baughn, J. W., Hoffman, M. A., and Takahashi, R. K., "Local Heat Transfer Downstream of an Abrupt Expansion in a Circular Channel with a Constant Wall Heat Flux," *Journal of Heat Transfer*, Vol. 106, No. 4, 1984, pp. 789–796. doi:10.1115/1.3246753

[21] Baughn, J. W., Hoffman, M. A., and Lee, D., "Heat Transfer Measurements Downstream of an Abrupt Expansion in a Circular Duct with a Constant Wall Temperature," *Papers Presented at the ASME Winter Annual Meeting*, Anaheim, CA, American Soc. of Mechanical Engineers, Fairfield, NJ, 1986, p. 7.

[22] Wong, D. H., Ireland, P. T., and Neely, A. J., "Preliminary Experiment Investigation of Acoustic Liner Heat Passing Capacity," 5th AIAA Aeroacoustics Conference, AIAA Paper 1999-1950, 1999.

[23] Wong, D. H., Ireland, P. T., and Neely, A. J., "An Experimental Investigation of Heat Transfer Through Acoustic Liner Panels in the Presence of a Crossflow," *ICAS 2000 CONGRESS*, ICAS, Europe, 2000.

[24] Wen, T., Tian, J., and Lu, T. J., "Forced Convection in Metallic Honeycomb Structures," *International Journal of Heat and Mass Transfer*, Vol. 49, Nos. 19–20, 2006, pp. 3313–3324. doi:10.1016/j.ijheatmasstransfer.2006.03.024

[25] Stein, J. M., and Dornfeld, D. A., "Burr Formation in Drilling Miniature Holes," *CIRP Annals: Manufacturing Technology*, Vol. 46, No. 1, 1997, pp. 63–66. doi:10.1016/S0007-8506(07)60776-8

[26] Kim, J., and Dornfeld, D. A., "Development of an Analytical Model for Drilling Burr Formation in Ductile Materials," *Journal of Engineering Materials and Technology*, Vol. 124, No. 2, 2002, pp. 192–198. doi:10.1115/1.1429937

[27] Lee, K., and Dornfeld, D. A., "Micro-Burr Formation and Minimization Through Process Control," *Precision Engineering*, Vol. 29, No. 2, 2005, pp. 246–252. doi:10.1016/j.precisioneng.2004.09.002

[28] Holman, J. P., *Heat Transfer*, 9th ed., McGraw–Hill, New York, 2002, pp. 232–239.

[29] Launder, B. E., and Spalding, D. B., "Numerical Computation of Turbulent Flows," *Computer Methods in Applied Mechanics and Engineering*, Vol. 3, No. 2, 1974, pp. 269–289. doi:10.1016/0045-7825(74)90029-2

[30] Guo, C., and Maxwell, W. H., "Turbulent Plane Jet Structure," *Journal of Engineering Mechanics*, Vol. 110, No. 10, 1984, pp. 1485–1497. doi:10.1061/(ASCE)0733-9399(1984)110:10(1485)

[31] Guo, C., and Maxwell, W. H., "Numerical Modelling of Normal Turbulent Plane Jet Impingement on Solid Wall," *Journal of Engineering Mechanics*, Vol. 110, No. 10, 1984, pp. 1498–1509. doi:10.1061/(ASCE)0733-9399(1984)110:10(1498)

[32] Schwarze, R., Klostermann, J., and Brucker, C., "Experimental and Numerical Investigations of a Turbulent Round Jet into a Cavity," *International Journal of Heat and Fluid Flow*, Vol. 29, No. 6, 2008, pp. 1688–1698. doi:10.1016/j.ijheatfluidflow.2008.08.001

[33] Cho, H. H., and Goldstein, R. J., "Heat (Mass) Transfer and Film Cooling Effectiveness with Injection Through Discrete Holes. Part II: On the Exposed Surface," *Proceedings of the ASME Winter Conference*, New Orleans, LA, American Soc. of Mechanical Engineers, Fairfield, NJ, 1993, pp. 1–12.

[34] Batchelor, G. K., *An Introduction to Fluid Dynamics*, 3rd ed., Cambridge Univ. Press, Cambridge, England, U.K., 2000, pp. 374–375.

[35] Ives, A. O., Wang, J., and Raghunathan, S., "Three Dimensional Numerical Solution of Heat Transfer in a Honeycomb Cell," 7th AIAA Aviation Technology, Integration, and Operations Conference, Belfast, Northern Ireland, U.K., AIAA, Paper 2007-7825, 2007.

[36] Moe, J. M., Wunsch, J. J., and Sperling, M. S., U.S. Patent Application for "Method and Apparatus for Noise Abatement and Ice Protection of an Aircraft Engine Nacelle Inlet Lip," Patent No. 20050006529, filed 13 Jan. 2005.

[37] Thomas, R. H., Choudhari, M. M., and Joslin, R. D., "Flow and Noise Control: Review and Assessment of Future Directions," NASA TM-2002-211631, 2002.